Modeling of the Magnetic Field-Induced Martensitic Variant Reorientation and the Associated Magnetic Shape Memory Effect in MSMAs

Björn Kiefer[a] and Dimitris C. Lagoudas[a]

[a] Department of Aerospace Engineering, Texas A&M University, H. R. Bright Building 3141 TAMU, College Station, TX 77843-3141 USA

ABSTRACT

This work is concerned with the magnetic field-induced rearrangement of martensitic variants in magnetic shape memory alloys (MSMAs). In addition to the variant reorientation, the rotation of the magnetization and magnetic domain wall motion are considered as the microstructural mechanisms causing the macroscopically observable constitutive response. The considered free energy terms are the elastic strain energy, the Zeeman energy and the magnetocrystalline anisotropy energy. It is shown how thermodynamic constraints on the magnetization rotation lead to only partial reorientation of the martensitic variants under higher stresses. A straightforward methodology has been devised for the calibration of model parameters based on experimental data. The presented model predictions indicate an improvement of the predictability of the nonlinear strain hysteresis and in particular the magnetization hysteresis.

Keywords: magnetic shape memory alloys, ferromagnetic shape memory effect, magnetic field induced strain, martensitic variant reorientation, magnetic hysteresis.

1. MAGNETIC SHAPE MEMORY ALLOYS AND THEIR APPLICATIONS

Magnetic shape memory alloys have been considered as alternative actuator materials to be used for applications not suitable for conventional shape memory alloys (SMAs). The high mobility of twin boundaries in the martensitic phase of MSMAs allows for high frequency magnetic actuation. Furthermore, because the deformation of the MSMA material is magnetic-field controlled, the actuation can in principle be initiated in a contact-free manner. A first generation of such actuators have been designed and built and are presently commercially available.[1–3]

Magnetic shape memory alloys (MSMAs) have intensely been researched since the first studies of their behavior were reported by Ullakko et al. (1996).[4] They found magnetic field-induced trains of nearly 0.2% in stress-free experiments on martensitic NiMnGa single crystals. Extensive experimental work on off-stoichiometric intermetallic compounds near the composition Ni_2MnGa have yielded of up to 10% in single crystals.[5] Additional alloys have been investigated, such as FePd[6,7] and CoNiAL,[8] among others. Under the influence of temperature and stress fields, MSMAs also exhibit conventional shape memory and pseudoelastic behavior.

The magnetic field-induced rearrangement of martensitic variants and the associated actuation of large inelastic strains has been termed the magnetic shape memory effect (MSME). The process occurs because each of the variants possesses different preferred directions of magnetization, called magnetic easy axes. That way those variants that are more favorably oriented with respect to an externally applied magnetic field can be selected over other less favorably oriented ones, resulting in the observed macroscopic shape change. The field-induced deformation of the material is accompanied by a nonlinear change in its magnetization, a process which will be discussed in more detail in the following section.

The phenomenological constitutive model proposed in this work addresses the constitutive behavior of MSMA in terms of the nonlinear and hysteretic strain and magnetization response of the MSMA material under applied mechanical loads and magnetic fields. The governing constitutive equations are derived from a free energy function with the help of thermodynamic restrictions. Having a functional constitutive model at the continuum

Further author information:
Contact Email: lagoudas@aero.tamu.edu

Smart Structures and Materials 2005: Active Materials: Behavior and Mechanics,Proceedings of SPIE Vol. 5761, 454–465.

scale is essential if one intends to design and analyze MSMA actuators and sensors, for example by utilizing finite element analysis. Micro-scale models that have been derived to describe the MSMA constitutive behaviour, although very useful in obtaining a fundamental understanding of the behavior of these materials on smaller scales, do not provide the capability to analyze life-sized components that are of interest to the actuator designing engineer. Furthermore, the model has a clearly defined set of parameters, which can uniquely be determined from a limited number of standard experiments as will be described in Section 4.

Various constitutive models have been presented in the literature, of which some of the most prominent have been proposed by James and Wuttig (1998)[9] and James and Hane (2000),[10] O'Handley (1998),[11] Likhachev and Ullakko (2000),[12] Hirsinger and Lexcellent (2003),[13] Glavatska et al. (2003)[14] and Muellner et al. (2003).[15] For a more detailed review of the literature on the modeling of MSMAs the reader is referred to Kiefer and Lagoudas (2005)[16] and Kiang and Tong (2005).[17] Most of the mentioned constitutive models rely on the minimization of an energy function, an approach which essentially assumes that there exists a perfectly conversion of magnetic into mechanical power. In this work the dissipative nature of the material behavior is taken into account by the introduction of internal state variables in the energy function. Furthermore, the model incorporates all three effects, the martensitic variant reorientation, the rotation of the magnetization and the magnetic domain wall motion as essential micro-scale mechanism which drive the macroscopically observed constitutive response.

The structure of the paper is as follows: Section 2 takes a closer look at the microstructural changes causing the described macroscopic constitutive behavior. This analysis is used as motivation for the formulation of the free energy function on which the constitutive model is based. The governing equations of the phenomenological continuum scale MSMA constitutive model are derived in Section 3. Section 4 explains the procedure devised to calibrate the model parameters on the basis of data obtained from standard experiments. Specific model parameters are deduced for published material data. The constitutive model is then applied to a special isobaric loading case in Section 5. Numerical predictions of strain and magnetization hysteresis curves are discussed in detail, with special emphasis on explaining the influence of the incorporated microstructural mechanisms on the macroscopic material response. It is also indicated how the proposed model has significantly improved the predictability of the magnetization hysteresis. The paper closes with the Discussion section, in which the important contributions of this work are summarized. As part of the future work efforts it is discussed how the constitutive model will be used in solving magneto-mechanical boundary value problems, which need to be solved in order to improve the design and analysis of MSMA actuators.

2. MICROSTRUCTURAL CONSIDERATIONS MOTIVATING THE CONSTITUTIVE MODELING APPROACH

The martensitic variant rearrangement process has been identified as the microstructural mechanism causing the large nonlinear magnetic field-induced strains in MSMA. In Ni_2MnGa, for example, the most commonly observed phase transformation is from the $L2_1$ Heusler type structured austenite to a tetragonal martensite structure. The three tetragonal variants are distinguished as variant 1, 2 and 3 by the alignment of their respective short axes c_i with the $[100], [010]$ and $[001]$ crystallographic directions of austenite, respectively.

The crystallographic rearrangement also changes the overall magnetization of the material, since the preferred magnetization directions differ between the martensitic variants. In the case of Ni_2MnGa the magnetic easy axes are aligned with the short axes of the tetragonal unit cells. Additional mechanisms that change the magnetization are the magnetic domain wall motion and the rotation of the magnetization away from the magnetic easy axes within magnetic domains. For a two-dimensional configuration a schematic view of the microstructure is shown in Figure 1. Depicted is the twinned arrangement of the variant 1 band, denoted by its volume fraction $(1-\xi)$, with the variant 2 band of volume fraction ξ. Each twin band is further divided into magnetic domains. Each domain is distinguished by the direction of its (spontaneous) magnetization. The volume fraction α denotes those domains whose magnetization vectors point in the positive coordinate directions. The magnetic easy axes of each domain are indicated by dashed lines. The rotation of the magnetization away from these preferred reference configurations is measured by the angles θ_i. It is evident from this configuration how the motion of twin boundaries (inclined lines), the motion of magnetic domain walls (horizontal and vertical lines) and the rotation of the magnetization vectors change the crystallographic and magnetic microstructure of the MSMA material. Multi-variant, multi-domain configurations of this type have in fact been observed experimentally.[18, 19]

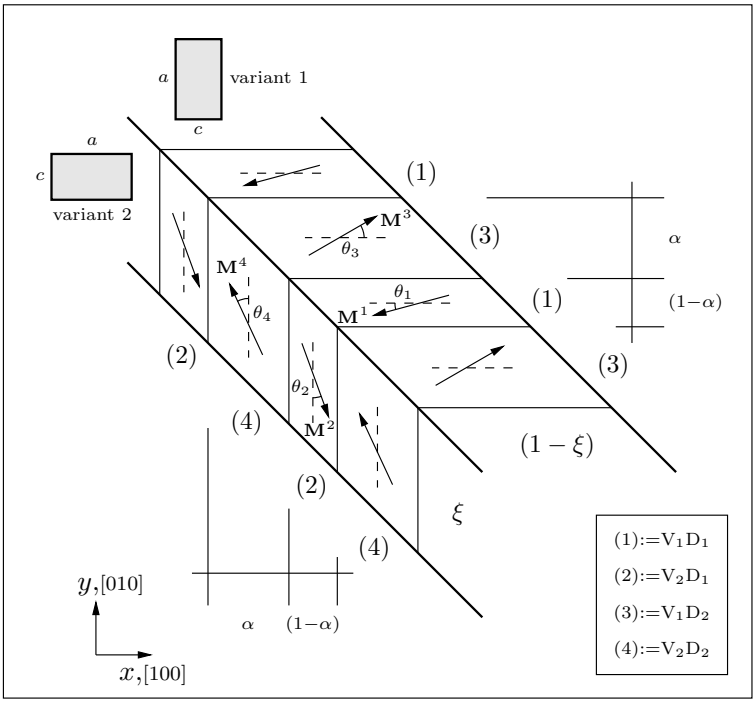

Figure 1. Coexistence of martensitic variants and magnetic domains at a twin boundary during the variant reorientation process. The angles θ_i measure the rotation of magnetization vectors with respect to the magnetic easy axes. The four distinct domains are numbered 1–4 to simplify the notation. The abbreviation V_1D_2, for example, stands for "variant 1, domain 2".

To connect these microstructural observations to the macroscopic material response, let us now consider the mechanical and magnetic loading of a MSMA single crystal in a setup which is typically used in the experimental investigation of the magnetic shape memory effect, as schematically shown in Figure 2.

The MSMA single crystal has been cooled under the application of a compressive axial stress to induce the martensitic transformation process and to guarantee an initial single variant 1 state (short c-axis along [100]). To simplify the analysis of the complex constitutive response to some degree, it is henceforth assumed that certain unfavorable magnetic domains are eliminated at relatively low applied magnetic field levels, an assumption which has been argued to be a good approximation of the observed behavior by other researchers.[5, 20] It should be remarked, however, that the most general form of the constitutive model presented here[16] does incorporate the motion of magnetic domain walls in general terms. The assumed fixed magnetic domain structure ($\alpha = 0$, if the external magnetic field is applied in the negative y-direction and $\alpha = 1$, for the positive y-direction) is also depicted in the schematics of Figure 2, which represent a sequence of special cases of the most general microstructural arrangement previously introduced in Figure 1.

If an external magnetic field is applied in the transverse direction the material initially responds only by rotating the magnetization in variant 1. When the external field is raised to a critical threshold level, the second variant is nucleated, since its preferred magnetic axis is aligned with this direction, while the magnetization rotation in variant 1 continuously increases. In the crystallographic rearrangement process, the short axis c of variant 1, which is aligned with the axial direction, is replaced by the long axis a of variant 2. The resulting axial strain is often approximated as $\varepsilon_{xx} = (a - c)/a$. When the rearrangement is completed by further increase of the applied magnetic field, the specimen consists entirely of variant 2 martensite and has attained the maximum possible reorientation strain. In the final configuration the material is also magnetized to saturation in the transverse direction.

The next section derives an appropriate constitutive model for the variant rearrangement process. One of its key ingredients is the free energy expression, which incorporates the microstructural mechanisms as motivated by the discussion in this section.

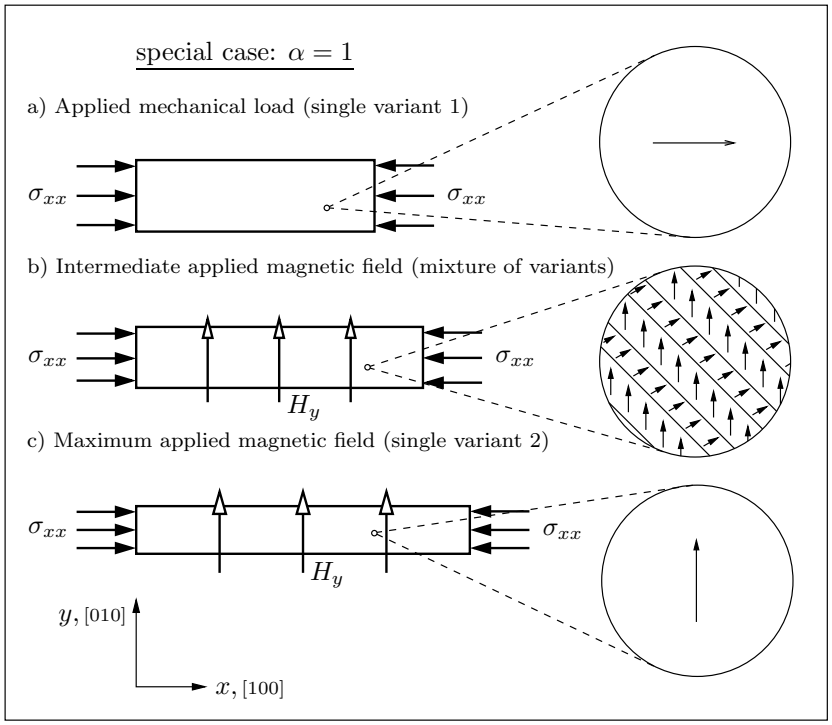

Figure 2. Special loading case for the magnetic field-induced variant rearrangement process.

3. GOVERNING MAGNETOMECHANICAL CONSTITUTIVE EQUATIONS

The Gibbs free energy function for the MSMA martensitic variant reorientation model has previously been proposed by the authors.[16, 21] Motivated by the analysis of possible energy contributions that are physically relevant for the magnetic shape memory effect, the elastic strain energy, the Zeeman energy, which aims to align the internal magnetization with the externally applied magnetic field, and the magnetic anisotropy energy are included in the free energy expression. The latter can be viewed as the energy difference associated with magnetizing a magnetic material along preferred and non-preferred directions, or in other words as the energy associated with the rotation of the magnetization away from the magnetic easy axes. These energy terms have also been included in other constitutive models.[10, 11, 13, 22] This paper, however, is concerned with the influence of dissipative effects in the evolution of thermodynamic states, rather than the minimization of the free energy, which searches for equilibrium points in ideal processes.

Under the assumption of a non-variable magnetic domain volume fraction ($\alpha = 1$) the Gibbs free energy for the constitutive model proposed here is given by

$$G = G(\boldsymbol{\sigma}, \mathbf{H}, \xi, \theta_i) = -\frac{1}{2\rho}\,\boldsymbol{\sigma} : \mathcal{S}(\xi)\boldsymbol{\sigma} - \frac{\mu_0}{\rho}\mathbf{M}(\xi, \theta_i)\cdot\mathbf{H} + G^{\mathrm{an}}(\xi, \theta_i) + \frac{1}{\rho}\, f^{\xi}(\xi) + G_0 \,, \tag{1}$$

where μ_0 is the permeability of free space and ρ is the mass density. The Cauchy stress tensor $\boldsymbol{\sigma}$ and the magnetic field strength vector $\mathbf{H}$ are the independent state variables, whereas the volume fraction ξ and the magnetization rotation angles θ_i are internal state variables. Note that the total Gibbs free energy Eq. (1) is constructed as a linear average of the contributions of each variant and corrected by the mixing term $f^{\xi}(\xi)$ and has a reference state value of G_0.[16, 21] The effective elastic compliance $\mathcal{S}$, effective magnetization $\mathbf{M}$ and effective magnetic anisotropy energy G^{an} are defined by

$$\begin{aligned} \mathcal{S} &= \mathcal{S}^{\mathrm{V}_1} + \xi\Delta\mathcal{S} = (1-\xi)\mathcal{S}^{\mathrm{V}_1} + \xi\mathcal{S}^{\mathrm{V}_2} \,, \\ \mathbf{M} &= (1-\xi)\mathbf{M}^{\mathrm{V}_1} + \xi\mathbf{M}^{\mathrm{V}_2} = (1-\xi)\mathbf{M}^{3} + \xi\mathbf{M}^{4} \,, \\ G^{\mathrm{an}} &= (1-\xi)G^{\mathrm{an},\mathrm{V}_1} + \xi G^{\mathrm{an},\mathrm{V}_2} = (1-\xi)G^{\mathrm{an},3}(\theta_3) + \xi G^{\mathrm{an},4}(\theta_4) \,. \end{aligned} \tag{2}$$

Recall that for the fixed magnetic domain case each variant is magnetized to the saturation value M^{sat} along the directions specified by the rotation angles θ_i measured with respect to the magnetic easy axes (cf. Figure 1). The anisotropy energy contributions by the individual magnetic domains $G^{\mathrm{an,i}}$ can, for an assumed *uniaxial symmetry*, be expressed as a series expansion of the form

$$G^{\mathrm{an,i}} = \sum_{n=1}^{N} K_n \sin^{2n}(\theta) \ , \tag{3}$$

of which only the first term is going to be considered in the computations presented in this paper.

From thermodynamic restrictions,[16] the following constitutive relations for the elastic strain $\boldsymbol{\varepsilon}^{\mathrm{e}}$, the magnetization $\mathbf{M}$, the driving force for variant reorientation π^{ξ} and the driving forces for magnetization rotation π^{θ_i}, are derived from the Gibbs free energy Eq. (1) as

$$\begin{aligned}
\boldsymbol{\varepsilon}^{\mathrm{e}} &:= -\rho\frac{\partial G}{\partial \boldsymbol{\sigma}} = \mathcal{S}\boldsymbol{\sigma} \ , \\
\mathbf{M} &:= -\frac{\rho}{\mu_0}\frac{\partial G}{\partial \mathbf{H}} = M^{\mathrm{sat}}(1-\xi)\big[\cos(\theta_3)\mathbf{e}_x + \sin(\theta_3)\mathbf{e}_y\big] + M^{\mathrm{sat}}\xi\big[-\sin(\theta_4)\mathbf{e}_x + \cos(\theta_4)\mathbf{e}_y\big] \\
\pi^{\xi} &:= \boldsymbol{\sigma}^{\mathrm{eff}} : \boldsymbol{\Lambda}^{\mathrm{r}} - \rho\frac{\partial G}{\partial \xi} = \boldsymbol{\sigma}^{\mathrm{eff}} : \boldsymbol{\Lambda}^{\mathrm{r}} + \frac{1}{2}\,\boldsymbol{\sigma} : \Delta\mathcal{S}\boldsymbol{\sigma} - \mu_0\Big[\mathbf{M}^3 - \mathbf{M}^4\Big]\cdot\mathbf{H} + \rho\Big[G^{\mathrm{an},3}(\theta_3) - G^{\mathrm{an},4}(\theta_4)\Big] - \frac{\partial f^{\xi}}{\partial \xi} \\
\pi^{\theta_3} &:= -\rho\frac{\partial G}{\partial \theta_3} = (1-\xi)\left[\mu_0 M^{\mathrm{sat}}\Big[-\sin(\theta_3)H_x + \cos(\theta_3)H_y\Big] - \rho\frac{\partial G^{\mathrm{an},3}}{\partial \theta_3}\right] \ , \\
\pi^{\theta_4} &:= -\rho\frac{\partial G}{\partial \theta_4} = \xi\left[\mu_0 M^{\mathrm{sat}}\Big[-\cos(\theta_4)H_x - \sin(\theta_4)H_y\Big] - \rho\frac{\partial G^{\mathrm{an},4}}{\partial \theta_4}\right] \ ,
\end{aligned} \tag{4}$$

where the definition of the effective stress tensor $\boldsymbol{\sigma}^{\mathrm{eff}} := \boldsymbol{\sigma} - \rho\frac{\partial G}{\partial \boldsymbol{\varepsilon}^{\mathrm{r}}}$ has been used.

It has further been assumed that the total strain can be additively decomposed into $\boldsymbol{\varepsilon} = \boldsymbol{\varepsilon}^{\mathrm{e}} + \boldsymbol{\varepsilon}^{\mathrm{r}} + \bar{\boldsymbol{\varepsilon}}^{\mathrm{off}}$, where $\boldsymbol{\varepsilon}^{\mathrm{r}}$ is the reorientation strain and $\bar{\boldsymbol{\varepsilon}}^{\mathrm{off}}$ is a strain offset, related to the deformations caused by the phase transformation prior to the application of the magnetic field in the martensitic state. This strain needs to be introduced since the undeformed austenite is taken a the reference configuration. The evolution of reorientation strain is proposed to be proportional to the rate of change of the martensitic volume fraction so that

$$\dot{\boldsymbol{\varepsilon}}^{\mathrm{r}} = \boldsymbol{\Lambda}^{\mathrm{r}}\dot{\xi} \ . \tag{5}$$

$\boldsymbol{\Lambda}^{\mathrm{r}}$ is the reorientation strain tensor defining the direction in which the reorientation strain develops. If $\boldsymbol{\Lambda}^{\mathrm{r}}$ is constant along the chosen loading path, Eq. (5) can be integrated to yield the reorientation strain, so that with Eq. (4a) the total strain is given by

$$\boldsymbol{\varepsilon} = \mathcal{S}\boldsymbol{\sigma} + \boldsymbol{\Lambda}^{\mathrm{r}}\xi + \bar{\boldsymbol{\varepsilon}}^{\mathrm{off}} \ . \tag{6}$$

From physical observations it is reasonable to assume that the magnetization rotations are thermodynamically reversible,[23] and thus do not contribute to the entropy production, which leads to the conclusion that the driving forces for the respective magnetization rotations are zero, i. e.

$$\pi^{\theta_i} := -\rho\frac{\partial G}{\partial \theta_i} = 0 \ . \tag{7}$$

These additional constraints are used to eliminate the explicit dependencies of the governing model equations on the magnetization rotation angles θ_i.

The thermodynamic restrictions placed on the martensitic variant rearrangement process can in this context be expressed by the simple Clausius-Duhem inequality[16]

$$\pi^{\xi}\dot{\xi} \geq 0 \ . \tag{8}$$

The rate independent nature of the model motivates the introduction of a reorientation function

$$\Phi^{\xi}(\boldsymbol{\sigma},\mathbf{H},\xi)=\begin{cases}\pi^{\xi}-Y^{\xi}\,, & \dot{\xi}>0\\ -\pi^{\xi}-Y^{\xi}\,, & \dot{\xi}<0\end{cases}\,, \tag{9}$$

which defines threshold values for the activation of the reorientation process that depend on the independent state variables. The thermodynamic restriction Eq. (8) placed on the reorientation process defined by Eq. (9) can be summarized in terms of the following Kuhn-Tucker reorientation conditions

$$\begin{aligned}&\dot{\xi}\geq 0, \quad \Phi^{\xi}(\boldsymbol{\sigma},\mathbf{H},\xi)\leq 0, \quad \Phi^{\xi}\dot{\xi}=0\,,\\ &\dot{\xi}\leq 0, \quad \Phi^{\xi}(\boldsymbol{\sigma},\mathbf{H},\xi)\leq 0, \quad \Phi^{\xi}\dot{\xi}=0\,.\end{aligned} \tag{10}$$

The presented model equations can further be reduced by considering the special loading conditions previously shown in Figure 2. The non-zero components of the applied magnetic field and applied stress are $H_y = H$, with $0 \leq H \leq H^{\mathrm{max}}$, and $\sigma_{xx} = \sigma$, with $\sigma < 0$, respectively. The reorientation tensor has the non-vanishing components $\Lambda^{\mathrm{r}}_{xx} = \varepsilon^{\mathrm{r,max}}$ and $\Lambda^{\mathrm{r}}_{yy} = -\varepsilon^{\mathrm{r,max}}$, for this two-dimensional case, so that the first term in Eq. (4c) is given by $\boldsymbol{\sigma}^{\mathrm{eff}}\!:\boldsymbol{\Lambda}^{\mathrm{r}} = \sigma\varepsilon^{\mathrm{r,max}}$.

For the specified loading case the Gibbs free energy and the resulting driving force for variant rearrangement Eqs. (4b) and (4c), respectively, reduce to the simpler expressions

$$\begin{aligned}G &= -\frac{1}{2\rho}S(\xi)\sigma^2-\frac{\mu_0}{\rho}M^{\mathrm{sat}}\big[(1-\xi)\sin(\theta_3)+\xi\cos(\theta_4)\big]H+K_1\big[(1-\xi)\sin^2(\theta_3)+\xi\sin^2(\theta_4)\big]+\frac{1}{\rho}f^{\xi}+G_0\,,\\ \pi^{\xi} &= \sigma\varepsilon^{\mathrm{r,max}}+\frac{1}{2}\Delta S\sigma^2-\frac{\mu_0}{\rho}M^{\mathrm{sat}}\big[\sin(\theta_3)-\cos(\theta_4)\big]H+\rho K_1\big[\sin^2(\theta_3)-\sin^2(\theta_4)\big]-\frac{\partial f^{\xi}}{\partial\xi}\,,\end{aligned} \tag{11}$$

The constraints (4d,e) are utilized to eliminate the rotation angles in Eqs. (11). For the rotation angle θ_3 it follows

$$\sin(\theta_3)=\frac{\mu_0 M^{\mathrm{sat}}}{2\rho K_1}H, \qquad \text{for } 0\leq\theta_3<\frac{\pi}{2} \text{ and } 0\leq\xi<1\,. \tag{12}$$

Since the magnetic field is applied in the y-direction, the corresponding constraint on θ_4 reflects the fact that the magnetization in variant 2, in this case, does not rotate away from the easy axis.

It is important to notice that according to Eq. (12) the magnetization in variant 1 has fully rotated ($\theta_3 = \frac{\pi}{2}$) at a critical magnetic field of $H^{\mathrm{crit}} = 2\rho K_1/\mu_0 M^{\mathrm{sat}}$. The driving force for twin boundary motion Eq. (11b) does then no longer depend on H. The reason is that when the magnetization is completely aligned with the applied magnetic field, the Zeeman energy difference across the twin boundary vanishes. Therefore, if the critical magnetic field value is below the finish point of the reorientation process for a given applied stress, variant 1 is not completely eliminated, even for high magnetic fields. This results in a reduced maximum reorientation strain produced in the hysteresis cycle under this particular stress. As a result of this upper limit for the reorientation strain evolution, which has been derived as a direct consequence of the introduction of the magnetization rotation, the martensitic volume fraction has to be reinterpreted. In the previous formulation of the model[16, 21] the martensitic volume fraction was considered to be an intrinsic normalized reorientation variable, always ranging from 0 to 1, while the maximum reorientation strain was introduced as stress dependent input data to the model. Here, the volume fraction ξ has the meaning of the physical volume fraction that can be measured in experiments, and the maximum reorientation strain is a given constant value, dictated by the crystal structure of the considered material. The numerical results presented in Section 5 will illustrate the impact of the discussed expanded model.

To complete the set of governing model equations a quadratic polynomial hardening function of the form

$$f^{\xi,\mathrm{p}}(\xi)=\begin{cases}\frac{1}{2}A^{\mathrm{p}}\xi^2+(B_1^{\mathrm{p}}+B_2^{\mathrm{p}})\xi\,, & \dot{\xi}>0\\ \frac{1}{2}C^{\mathrm{p}}\xi^2+(B_1^{\mathrm{p}}-B_2^{\mathrm{p}})\xi\,, & \dot{\xi}<0\end{cases}\,, \tag{13}$$

which yields

$$\frac{\partial f^{\xi,\mathrm{p}}}{\partial \xi} = \begin{cases} A^{\mathrm{p}}\xi + B_1^{\mathrm{p}} + B_2^{\mathrm{p}}\,, & \dot{\xi} > 0 \\ C^{\mathrm{p}}\xi + B_1^{\mathrm{p}} - B_2^{\mathrm{p}}\,, & \dot{\xi} < 0 \end{cases}\,, \tag{14}$$

is introduced, where $A^{\mathrm{p}}, B_1^{\mathrm{p}}, B_2^{\mathrm{p}}$ and C^{p} are adjustable parameters of the quadratic polynomial hardening function. It has been shown[16, 24] that other functions may be more suitable to reflect the nature of the reorientation strain hardening observed in experiments. However, the quadratic polynomial, which leads to a linear hardening behavior, is utilized here to demonstrate the impact of the nonlinearities introduced by the magnetization rotation. It will be shown in Section 4, how the hardening parameters can be connected to physically measurable quantities.

4. THE CALIBRATION OF THE MODEL PARAMETERS

If the mass density ρ and the difference in elastic compliance between the long and short axis directions of the tetragonal martensitic crystal ΔS are known, seven additional data points are needed to calibrate the constitutive model, which can be determined from two experiments to be identified. Experiment 1: Measurement of the magnetization along the hard axis and easy axis of a constrained MSMA single crystal, in which the reorientation process is completely suppressed by the application of a compressive stress higher than the blocking stress. The resulting data is used to determine the saturation magnetization M^{sat}, and the magnetocrystalline anisotropy energy ρK_1. The latter is obtained by evaluating the area between the measured magnetization curves. Experiment 2: Measurement of one strain hysteresis loop, preferably at a stress level under which a complete reorientation of variants in which full strain is obtained, to find the magnitude of the maximum reorientation strain $\varepsilon^{\mathrm{r,max}}$, and estimate the magnetic field threshold values for the start and finish of the forward rearrangement process (variant 1 $\rightarrow$ variant 2), denoted $H^{\mathrm{s}(1,2)}$ and $H^{\mathrm{f}(1,2)}$, and the corresponding values for the reverse process (variant 2 $\rightarrow$ variant1) $H^{\mathrm{s}(2,1)}$ and $H^{\mathrm{f}(2,1)}$.

$$\begin{aligned}
A^{\mathrm{p}} &= \mu_0 M^{\mathrm{sat}}\big(H^{\mathrm{f}(1,2)} - H^{\mathrm{s}(1,2)}\big) - \tfrac{(\mu_0 M^{\mathrm{sat}})^2}{4\rho K_1}\Big[(H^{\mathrm{f}(1,2)})^2 - (H^{\mathrm{s}(1,2)})^2\Big] \\
B_1^{\mathrm{p}} &= \tfrac{1}{2}\mu_0 M^{\mathrm{sat}}\big(H^{\mathrm{s}(1,2)} + H^{\mathrm{f}(2,1)}\big) - \tfrac{(\mu_0 M^{\mathrm{sat}})^2}{8\rho K_1}\Big[(H^{\mathrm{s}(1,2)})^2 + (H^{\mathrm{f}(2,1)})^2\Big] + \sigma^*\,\varepsilon^{\mathrm{r,max}} \\
B_2^{\mathrm{p}} &= \tfrac{1}{4}\big(C^{\mathrm{p}} - A^{\mathrm{p}}\big) \\
C^{\mathrm{p}} &= \mu_0 M^{\mathrm{sat}}\big(H^{\mathrm{s}(2,1)} - H^{\mathrm{f}(2,1)}\big) - \tfrac{(\mu_0 M^{\mathrm{sat}})^2}{4\rho K_1}\Big[(H^{\mathrm{s}(2,1)})^2 - (H^{\mathrm{f}(2,1)})^2\Big] \\
Y^{\xi,\mathrm{p}} &= \tfrac{1}{2}\mu_0 M^{\mathrm{sat}}\big(H^{\mathrm{s}(1,2)} - H^{\mathrm{f}(2,1)}\big) - \tfrac{(\mu_0 M^{\mathrm{sat}})^2}{8\rho K_1}\Big[(H^{\mathrm{s}(1,2)})^2 - (H^{\mathrm{f}(2,1)})^2\Big] - B_2^{\mathrm{p}}
\end{aligned}$$

Table 1. Relations between material constants and model parameters.

Once these seven input data have been identified the model calibration is completed by computing the hardening and hysteresis parameters A^{p},B_1^{p},B_2^{p},C^{p} and $Y^{\xi,\mathrm{p}}$ using the relations listed in Table 1, which have been derived from the evaluation of the constitutive equations (9), (10), (11b), (12) and (14) at the critical magnetic field levels with the respective variant volume fractions of $\xi = 0$ and $\xi = 1$.

This methodology has been employed to calibrate the hardening and hysteresis parameters for the numerical example to be presented in the following section, on the basis of experimental data reported by Heczko et al. 2003.[25] The input data and the resulting parameters are listed in Table 2.

5. PREDICTION OF THE MAGNETIC FIELD-INDUCED STRAIN AND MAGNETIZATION HYSTERESIS UNDER ISOBARIC CONDITIONS

For the considered special case numerical predictions of the reorientation strain-magnetic field-hysteresis loops have been computed, based on the parameters presented in the previous section, by substituting Eq. (14) into the

Material Parameters	
ρ	$8000.0\,\mathrm{kg\,m^{-3}}$
ρK_1	$1.67{\cdot}10^5\,\mathrm{Jm^{-3}}$
M^{sat}	$514.0{\cdot}10^3\,\mathrm{Am^{-1}}$
σ^*	$-1.0\,\mathrm{MPa}$
$\varepsilon^{\mathrm{r,max}}$	0.062
ΔS	0.0
$\mu_0 H^{\mathrm{s}(1,2)}$	0.35 T
$\mu_0 H^{\mathrm{f}(1,2)}$	0.6 T
$\mu_0 H^{\mathrm{s}(2,1)}$	0.32 T
$\mu_0 H^{\mathrm{f}(2,1)}$	-0.08 T

Hardening Parameters	
A^{p}	0.034568 MPa
B_1^{p}	-0.018100 MPa
B_2^{p}	0.033266 MPa
C^{p}	0.167632 MPa
Hysteresis Parameter	
$Y^{\xi,\mathrm{p}}$	0.054285 MPa

Table 2. Material parameters for the considered Ni_2MnGa specimen, and the resulting hardening and hysteresis parameters.

expression for the twin boundary motion driving force Eq. (11b) and satisfying the constraints Eq. (9), Eq. (10) and Eq. (12). The evolution of reorientation strain under different applied stress levels is shown in Figure 3.

Recall that the model parameters were determined from the strain curve at -1.0 MPa published in Heczko et. al. 2003,[25] which is shown as the dashed line in Figure 3. The the corresponding numerical hysteresis loop (solid line) therefore has to be considered a simulation of the input data, while the loops at the other two considered stress levels are model predictions. It is evident that the simulated loop at -1.0MPa represents a good approximation of the experimental data, with the exception of the inaccuracies at high magnetic fields. Some of these discrepancies can be eliminated by choosing more appropriate hardening functions than the quadratic polynomial (13) chosen for here. But further analysis is necessary to determine whether this trend in the evolution of the reorientation strain is consistent with other experimental evidence, or if there exist additional microstructural mechanism that have not yet been considered.

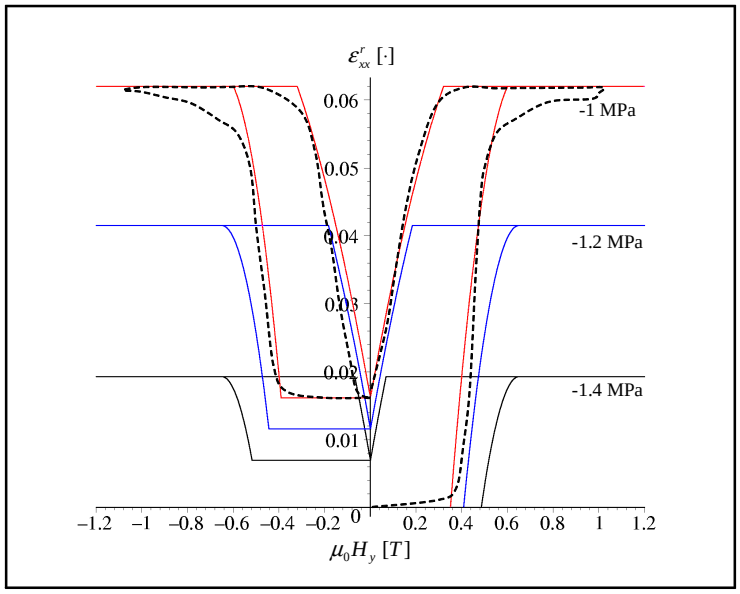

Figure 3. Axial reorientation strain vs. transversely applied magnetic field for different bias stress levels. Numerical results—solid lines, experimental data (-1.0 MPa)—dashed line.

Experiments have also shown that there exists a first cycle effect, in which the reorientation strain produced under the application of magnetic fields in the positive transverse direction is larger than the strain produced in following negative cycle.[20, 26] The reduced maximum strain value stabilizes for subsequent cycles. This effect is captured by the model predictions, as evident from Figure 3, by enforcing the condition that the evolution of the volume fraction is terminated when the rotation of the magnetization in variant 1 is complete.

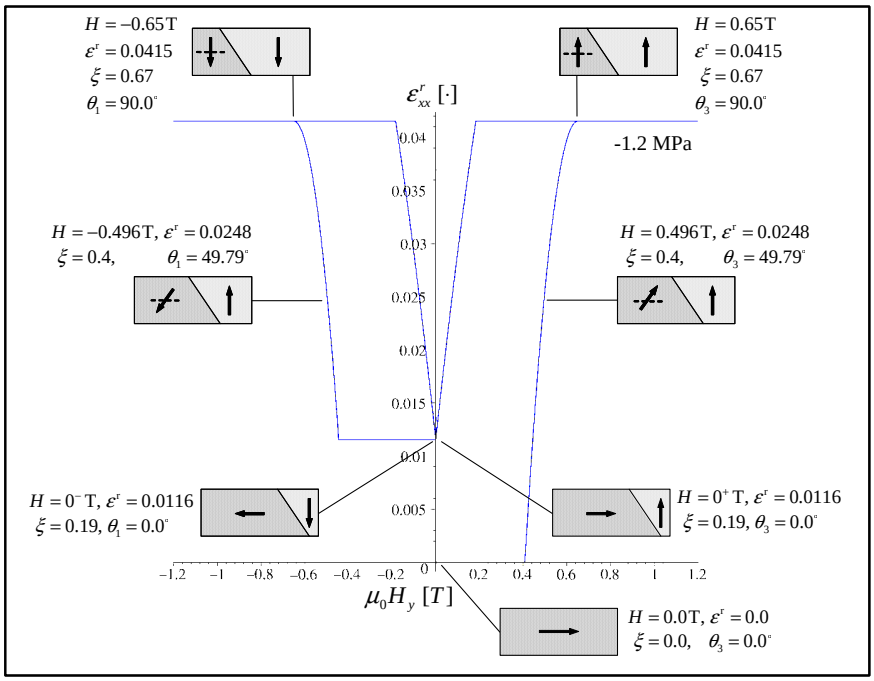

Figure 4. Schematic illustration of the evolution of the variant volume fraction and the magnetization rotation for the predicted hysteresis loop under −1.2 MPa.

In order to gain more physical inside into the evolution of the reorientation strain, with the concurrently developing variant rearrangement and magnetization rotation, Figure 4 takes a closer look at the predicted strain hysteresis loop under −1.2 MPa, that was previously shown in Figure 3.

Under the axial bias stress the MSMA specimen is initially in a single variant 1 state (see schematic in Figure 4). Following the proposition that the magnetic domain wall motion eliminates the less favorable of the two possible magnetic domains at low applied magnetic fields, the model predictions assumes the single domain configuration shown at 0.0 T. When the magnetic field is applied and has reached the critical threshold value of 0.408 T the reorientation process is initiated. At an applied magnetic field of 0.496 T, for example, 40% of the second variant has been produced, resulting in a reorientation strain of 2.48%, while the magnetization has rotated by 49.79°. For this particular example the critical magnetic field for complete rotation of the magnetization in variant 1 is $\mu_0 H^{\text{crit}} = 0.650\,\text{T}$, at which point 67% of variant 2 has developed, leading to a strain of 4.15%. Recall that further increase of the magnetic field can not result in an increase of the volume fraction since the driving force for twin boundary motion, as governed by Eq. (11b), no longer depends on the magnitude of the applied magnetic field. Furthermore it is evident from Figure 3 that the strain hysteresis at −1.4 MPa is terminated at a lower volume fraction, resulting in a lower achieved reorientation strain, while in the −1.0 MPa case the full strain develops, since the termination magnetic field value for the forward reorientation process is lower than the critical field. In other words, at −1.0 MPa variant 1 is eliminated before its magnetization has fully rotated.

When, by lowering the applied magnetic field, the threshold value for the reverse transformation is reached at 0.184 T, the second variant is decreased, as indicated in Figure 4. However, as the field approaches zero, the backward reorientation process is not completed, since the magnetization of the variants is reversed upon applying a negative magnetic field. In reality this process occurs by reversible domain wall motion. Since the model has been restricted in this special case to assume fixed domain configurations ($\alpha = \{0, 1\}$), the reversal of

the magnetization occurs instantaneously when the strain axis is crossed. The residual variant volume fraction for the considered −1.2 MPa curve is 19% and the strain is 1.16%. During the described reverse reorientation process, the magnetization in variant 1 rotates back to its reference orientation as the externally applied magnetic field is removed.

Although starting from different initial variant 1 volume fractions, the reorientation strain in the negative cycle evolves in a manner, which is analogous to that of the positive cycle, due to the symmetric nature of the assumed reorientation potential Eq. (9) and the hardening function Eq. (13). The residual strain at the end of the negative cycle is again 19%, so that the strain difference between initial and final configurations, as reflected in the height of the hysteresis loop, is given by 2.99%, which is lower than the 4.15% of the positive cycle. It should be clear that if the negative magnetic field had been applied first, a subsequent positive cycle would then exhibit the reduced reorientation strain, so that the hysteresis loop would appear as the mirror image of that of the presented case.

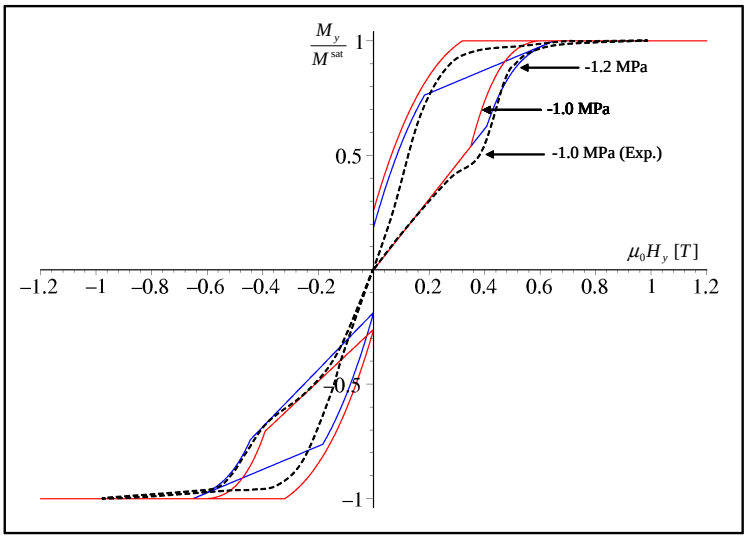

Figure 5. Transverse magnetization vs. transversely applied magnetic field for different bias stress levels. Numerical results—solid lines, experimental data (−1.0 MPa)—dashed line.

The effect of the simultaneous evolution of the volume fraction and the rotation of the magnetization is also clearly observable in the numerical transverse magnetization curves depicted in Figure 5. Note that both of the depicted curves represent model predictions, since all the needed material parameters where obtained from the strain hysteresis loop and magnetic measurements of the *constraint* single crystal. The −1.4 MPa curve has been omitted to avoid an overload of the depicted graph. Consider then the magnetization curve at the applied stress of −1.2 MPa, for which the corresponding strain hysteresis loop has just been analyzed in detail. For applied magnetic field levels below the threshold value of variant 2 nucleation, the magnetization process occurs along the hard axis of variant 1, by the mechanism of magnetization rotation. Because only the first term in the expansion of the anisotropy energy Eq. (3) has been considered, the magnetization (2b) has a linear dependence on H in this region. From Eqs. (2b) and (12), the slope is calculated to be $1.54\, M^{\text{sat}}$ [A/(mT)], a result which is in good agreement with the experimental data (dashed line) as measured by Heczko et. al. 2003.[25] When the nucleation of variant 2 sets in at 0.408 T, the change in magnetization is not only influenced by the continuously increasing rotation of the magnetization in variant 1, but is additionally driven by the magnetization of variant 2. This leads to the abrupt slope change of the magnetization curve, which is also observed in the experimental data. The influence of the variant 2 magnetization becomes more prominent as the reorientation process progresses.

As discussed in the context of the strain hysteresis in Figure 3, the evolution of the variant volume fraction is terminated as the magnetization in variant 1 is fully rotated. The material has then reached its saturation magnetization in the direction of the applied magnetic field. Since the forward reorientation process has not been completed, there exists a residual variant 1 volume fraction, which starts to reduce its magnetization upon

decrease of the applied magnetic field, resulting again in a linear variation of the magnetization. The slope, however, is different from the one initially observed for variant 1 at a low magnetic field level, since 67% of the material still consists of variant 2, whose magnetization remains unaffected by the decrease of the magnetic field. Another abrupt nonlinear variation of the magnetization occurs when the reverse transformation is activated at 0.184 T. Recall that at 0.0 T the residual variant 2 volume fraction is 19%, and the effective magnetization in the transverse direction is thus non-zero, even though the magnetization in variant 1 has rotated back to its reference configuration.

It is observed, that the prediction of the magnetization hysteresis in the region of the reverse reorientation is not quite as accurate as that of the forward process. Note in particular the jump of the magnetization curve as the applied field transitions from the positive to the negative transverse direction. This discontinuity is a direct consequence of the assumed fixed domain configuration. In reality domain wall motion processes ensure a vanishing macroscopic magnetization as the external magnetic field is removed, leading to a large, but finite slope of the magnetization curve as evident from the experimental data. This also leads to the observed offset of the negative numerical magnetization hysteresis. However, it should be concluded, that the assumption of fixed domain configurations yields reasonable results in the prediction of the magnetization curves. This is especially valid if one considers the fact that for the first time have such slope changes in the nonlinear magnetization hysteresis been predicted by a MSMA constitutive model.

6. DISCUSSION

A phenomenological constitutive model for the magnetic shape memory effect has been introduced on the basis of a free energy function, which incorporates the elastic strain energy, the Zeeman energy and the magnetic anisotropy energy. The dissipative nature of the variant reorientation process has been accounted for by the introduction of the martensitic variant volume fraction, the magnetic domain volume fraction and the magnetization rotation angles, as internal state variables. Their evolution has been proposed to be driven by the micro-scale mechanisms of twin boundary motion, magnetic domain wall motion and rotation of the magnetization. A methodology has been devised to calibrate the model parameters from clearly defined experimental data. The presented numerical results involving the strain and magnetization hysteresis, have illustrated that the model predicts the following important features: a) the stress dependence of the hysteresis shape. b) the variation of the induced reorientation strain from the first to the second cycle. c) the limiting effect of full magnetization rotation on the reorientation strain.

In future efforts, the model will be implemented into a finite element code, which has the capability of solving the coupled Maxwell's equations of magnetostatics and those of classical continuum mechanics. The magneto-mechanical coupling has two sources, namely the nonlinear hysteretic constitutive behavior, but also the fact that magnetic body forces and body couples enter the mechanical equations. The finite element analysis can then be used in the investigation of such effects as the specimen shape and size dependence, in magnetic shape memory effect experiments, in particular the influence of the demagnetization field and is thus expected to improve the interpretability of experimental data and consequently the design of MSMA actuators.

ACKNOWLEDGMENTS

This work was supported by the Army Research Office, contract no. DAAD 19-02-1-0261 and the National Science Foundation, award no. CMS-0324537.

REFERENCES

1. AdaptaMat Ltd., "MSM actuators." www.adaptamat.com, 2005.
2. I. Suorsa, E. Pagounis, and K. Ullakko, "Magnetic shape memory actuator performance," *Journal of Magnetism and Magnetic Materials* **272–276**, pp. 2029–2030, 2004.
3. MIDÉ Technology Corporation, "Ferromagnetic SMA actuator." www.mide.com, 2005.
4. K. Ullakko, J. K. Huang, C. Kantner, R. C. O'Handley, and V. V. Kokorin, "Large magnetic-field-induced strains in Ni_2MnGa single crystals," *Applied Physics Letters* **69**(13), pp. 1966–1968, 1996.

5. R. C. O'Handley, S. M. Allen, D. I. Paul, C. P. Henry, M. Marioni, D. Bono, C. Jenkins, A. Banful, and R. Wager, "Keynote address: Magnetic field-induced strain in single crystal Ni-Mn-Ga," *Proceedings of SPIE, Symposium on Smart Structures and Materials* **5053**, pp. 200–206, 2003.
6. J. Cui, T. W. Shield, and R. D. James, "Phase transformation and magnetic anisotropy of an iron-palladium ferromagnetic shape-memory alloy," *Acta Materialia* **52**, pp. 35–47, 2004.
7. T. Yamamoto, M. Taya, Y. Sutou, Y. Liang, T. Wada, and L. Sorensen, "Magnetic field-induced reversible variant rearrangement in Fe-Pd single crystals," *Acta Materialia* **52**(17), pp. 5083–5091, 2004.
8. H. E. Karaca, I. Karaman, Y. I. Chumlyakov, D. C. Lagoudas, and X. Zhang, "Compressive response of a single crystalline CoNiAl shape memory alloy," *Scripta Materialia* **51**, pp. 261–266, 2004.
9. R. D. James and M. Wuttig, "Magnetostriction of martensite," *Philosophical Magazine A* **77**(5), pp. 1273–1299, 1998.
10. R. D. James and K. F. Hane, "Martensitic transformations and shape-memory materials," *Acta Materialia* **48**(1), pp. 197–222, 2000.
11. R. C. O'Handley, "Model for strain and magnetization in magnetic shape-memory alloys," *Journal of Applied Physics* **83**(6), pp. 3263–3270, 1998.
12. A. A. Likhachev and K. Ullakko, "Magnetic-field-controlled twin boundaries motion and giant magneto-mechanical effects in Ni-Mn-Ga shape memory alloy," *Physics Letters A* **275**, pp. 142–151, 2000.
13. L. Hirsinger and C. Lexcellent, "Internal variable model for magneto-mechanical behaviour of ferromagnetic shape memory alloys Ni-Mn-Ga," *Journal de Physique IV* **112**, pp. 977–980, 2003.
14. N. I. Glavatska, A. A. Rudenko, I. N. Glavatskiy, and V. A. L'vov, "Statistical model of magnetostrain effect in martensite," *Journal of Magnetism and Magnetic Materials* **265**(2), pp. 142–151, 2003.
15. P. Müllner, V. A. Chernenko, and G. Kostorz, "A microscopic approach to the magnetic-field-induced deformation of martensite (magnetoplasticity)," *Journal of Magnetism and Magnetic Materials* **267**, pp. 325–334, 2003.
16. B. Kiefer and D. C. Lagoudas, "Magnetic field-induced martensitic variant reorientation in magnetic shape memory alloys," *To be published in Philosophical Magazine: Special Issue in Honor of SES 2003 Eringen Medalist G. Maugin* , pp. xxx–xxx, 2005.
17. J. Kiang and L. Tong, "Modelling of magneto-mechanical behavior of Ni-Mn-Ga single crystals," *Journal of Magnetism and Magnetic Materials* **292**, pp. 394–412, 2005.
18. A. A. Likhachev, A. Sozinov, and K. Ullakko, "Optimizing work output in Ni-Mn-Ga and other ferromagnetic shape memory alloys other ferromagnetic shape-memory alloys," *Proceedings of SPIE, Symposium on Smart Structures and Materials* **4699**, pp. 553–563, 2002.
19. M. R. Sullivan and H. D. Chopra, "Temperature- and field-dependent evolution of micromagnetic structure in ferromagnetic shape-memory-alloys," *Physical Review B* **70**, pp. 094427–(1–8), 2004.
20. R. Tickle, *Ferromagnetic Shape Memory Materials*. PhD thesis, University of Minnesota, May 2000.
21. B. Kiefer and D. C. Lagoudas, "Phenomenological modeling of ferromagnetic shape memory alloys," *Proceedings of SPIE, Smart Structures and Materials: Active Materials: Behavior and Mechanics, San Diego, CA, 14–18 March 2004* **Vol. 5387**, pp. 164–176, 2004.
22. T. W. Shield, "Magnetomechanical testing machine for ferromagnetic shape-memory alloys," *Review of Scientific Instruments* **74**(9), pp. 4077–4088, 2003.
23. B. D. Cullity, *Introduction to Magnetic Materials*, Addison-Wesley, 1972.
24. J. G. Boyd and D. C. Lagoudas, "A thermodynamical constitutive model for shape memory materials. Part I. The monolithic shape memory alloy," *International Journal of Plasticity* **12**(6), pp. 805–842, 1996.
25. O. Heczko, L. Straka, and K. Ullakko, "Relation between structure, magnetization process and magnetic shape memory effect of various martensites occuring in Ni-Mn-Ga alloys," *Journal de Physique IV* **112**, pp. 959–962, 2003.
26. I. Karaman, "Thermo-magneto-mechanical characterization and testing of MSMA single crystals, conducted at Texas A&M University, Departments of Aerospace Engineering and Mechanical Engineering." Internal Correspondence, 2004.